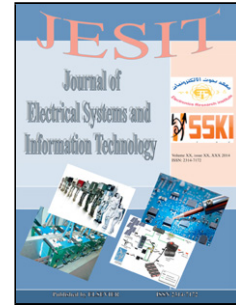


## Accepted Manuscript

Title: Wind Turbine Emulation Using Permanent Magnet Synchronous Motor

Authors: Mohamed E. Abdallah, Osama M. Arafa, Adel Shaltot, Ghada A. Abdel Aziz



PII: S2314-7172(18)30031-X  
DOI: <https://doi.org/10.1016/j.jesit.2018.03.005>  
Reference: JESIT 202

To appear in:

Received date: 31-12-2017  
Accepted date: 12-3-2018

Please cite this article as: Mohamed E.Abdallah, Osama M.Arafa, Adel Shaltot, Ghada A.Abdel Aziz, Wind Turbine Emulation Using Permanent Magnet Synchronous Motor (2018), <https://doi.org/10.1016/j.jesit.2018.03.005>

This is a PDF file of an unedited manuscript that has been accepted for publication. As a service to our customers we are providing this early version of the manuscript. The manuscript will undergo copyediting, typesetting, and review of the resulting proof before it is published in its final form. Please note that during the production process errors may be discovered which could affect the content, and all legal disclaimers that apply to the journal pertain.

# Wind Turbine Emulation Using Permanent Magnet Synchronous Motor

Mohamed E. Abdallah, Osama M. Arafa, Adel Shaltot, Ghada A. Abdel Aziz

Power Electronic Department, Electronics Research Institute, Egypt, eng.msa12@eri.sci.eg,  
Power Electronic Department, Electronics Research Institute, Egypt, oarafa2004@yahoo.com,  
Electric Power and Machines, Department, Cairo University, Egypt, aashaltout@yahoo.com  
Power Electronic Department, Electronics Research Institute, Egypt ghada\_ahmed@eri.sci.eg

**Abstract**—In wind energy conversion systems (WECS), the turbine captures part of the wind energy and converts it to mechanical energy through a dynamic interaction with the electrical generator which in turn converts this mechanical energy to electrical energy. Therefore, the dynamics of the wind turbine is very important in research and development of the overall WECS. Having a real wind turbine or a site with convenient wind conditions is not always a guaranteed option for conducting research. Hence, it is very desirable to create wind turbine dynamics through wind turbine emulation. In this paper, a wind turbine emulation system using a permanent magnet synchronous motor (PMSM) is designed, simulated, implemented, and tested experimentally. The PMSM is torque-controlled using field orientation technique. A three-phase IGBT inverter with closed loop current PI-controllers is used to drive the PMSM. A dSPACE DS1104 DSP prototyping platform is used to handle the real-time execution of the control programs. The system is tested and the torque-speed characteristics of the emulated wind turbine are verified experimentally at different feeds of wind speeds and generator loads.

**Index Terms**—Wind energy conversion system, wind turbine emulator, PMSM control.

## I. INTRODUCTION

A wind turbine emulator (WTE) is an equipment which is used for producing a real wind turbine characteristics in the laboratory. This emulator emulates the dynamic and static behavior of the real wind turbine without the need of natural wind resource and actual wind turbine.

For the purpose of research tests, a system is designed to emulate the wind turbine characteristics. The emulator can be coupled with an electrical generator to compose a complete wind energy conversion system (WECS) in a similar way like an actual wind turbine by generating torque similar to the aerodynamic torque at a given wind speed. Obviously, more control and flexibility are provided using emulators since selectable wind profiles, speeds and repeatable testing conditions can be conducted easily as desired without the need to a natural wind resource or too expensive wind turbine equipment. Squirrel cage induction motor (SCIM), permanent magnet synchronous motor (PMSM) and DC motor are usually used for emulating wind turbines in the laboratory [1]-[7]. These motors are controlled to have power curves similar to the wind turbine characteristics.

In this paper, a PMSM is selected to implement the emulation. The paper explains in sufficient details the different aspects of the implementation as follows: section II presents the wind turbine mathematical model. Sections III and IV give the details of PMSM control using field orientation technique including the design procedure of the PI current controllers. In section V, the experimental setup is described and the system testing results including the verification of the torque-speed characteristics of the emulated turbine and the experimental results of some testing scenarios are presented. Section VI provides the conclusion of this paper.

## II. WIND TURBINE MODEL

The wind turbine is the crucial mover of the WECS. Thus, the modeling of wind power is vital in studying and improving WECS. The mechanical output power of the wind turbine is given by (1) [8].

$$P_m = \frac{1}{2} \rho \pi R^2 C_p(\lambda, \beta) v_w^3 \quad (1)$$

where  $\rho$  is the air density in ( $\text{Kg/m}^3$ ),  $R$  is the radius of the rotor's swept area in (m),  $C_p$  is the power coefficient and  $v_w$  is the wind speed in (m/sec). The power coefficient is defined as the ratio of the turbine mechanical power to the power available by the wind. This coefficient is a function of  $TSR$  ( $\lambda$ ) and the pitch angle of the blades ( $\beta$ ) in (deg). The  $TSR$  is the ratio of the blade tip-speed divided by the wind speed as illustrated in (2).

$$\lambda = \frac{\omega_t R}{v_w} \quad (2)$$

where  $\omega_t$  is the rotor angular speed in (rad/sec).

The aerodynamic mechanical torque of the wind turbine is given by (3):

$$T_m = \frac{1}{2} \frac{\rho \pi R^3 C_p(\lambda, \beta) v_w^2}{\lambda} \quad (3)$$

As pointed in [9], the power coefficient,  $C_p(\lambda, \beta)$ , is a non-linear function of the tip speed ratio,  $\lambda$ , and the blade pitch angle,  $\beta$ . The  $C_p(\lambda, \beta)$  curve is specific characteristics of each wind turbine design and can be derived from a field test of the turbine. An empirical equation is normally used to model the  $C_p, \lambda$  and  $\beta$  surface, based on the turbine characteristics, as illustrated in (4), [1]-[3], [10].

$$C_p(\lambda, \beta) = C_1 \cdot \left( C_2 \cdot \frac{1}{\lambda_i} - C_3 \cdot \beta - C_4 \right) e^{\frac{C_5}{\lambda_i}} + C_6 \cdot \lambda \quad (4)$$

where the parameters  $C_1$  to  $C_6$  are constants and  $\lambda_i$  is given by (5):

$$\frac{1}{\lambda_i} = \frac{1}{\lambda + 0.08\beta} - \frac{0.035}{\beta^3 + 1} \quad (5)$$

Table I gives typical values of the parameters  $C_1$  to  $C_6$  [2]. These parameters vary from one turbine to another based on the aerodynamic characteristics of the turbine. Fig. 1 shows the power coefficient characteristic for different values of  $\lambda$  and  $\beta$  of the turbine with the parameters shown in Table I. For the set of parameters of Table I, the maximum theoretical value of the power coefficient ( $C_p = 0.48$ ) is achieved at  $\beta = 0$  deg. and  $\lambda = 8.108$ . Also, Fig. 2 shows the power coefficient curve at  $\beta = 0$ .

From the wind turbine power and torque in (1) and (3), it can be noticed that the inputs are the wind speed, the blades pitch angle and the rotor speed and the output is the aerodynamic torque. As a result, the wind turbine model or emulator must receive the same set of inputs and issues the same aerodynamic torque produced at each instant by the real turbine at the given specific inputs.

The role of the control applied to the used motor (DC, PMSM or SCIM) is to generate the commanded torque that would be issued by the given inputs from the real turbine. This torque is calculated in the control program in real time according to the characteristics embedded in the wind turbine model and the measured inputs. The complete strategy is illustrated in Fig. 3. The torque scaling factor,  $S_t$ , is used when the wind turbine ratings are higher than the emulating machine rating. The value of  $S_t$  is given by (6). Scaling eases the reproduction of the actual turbine aerodynamic characteristics but on the used machine scale to evade possible damage.

$$S_t = \frac{P_{\text{machine}}}{P_{\text{turbine}}} \quad (6)$$

where  $P_{\text{machine}}$  is the nominal power of the motor and  $P_{\text{turbine}}$  is the nominal turbine power.

The Simulink model of the 3 KW wind turbine is depicted in Fig. 4. This model is developed by (1)-(5) with  $R = 1.5$  m and  $\rho = 1$  Kg/m<sup>3</sup>.

### III. EMULATION OF WIND TURBINE DYNAMICS USING PMSM

A one KW surface-mounted PMSM is used to emulate the turbine characteristics mentioned in the previous section. The PMSM is controlled to track the torque command given by the wind turbine at any given set of inputs (e.g. wind speed, blade pitch angle, and measured rotor speed). To obtain high-performance torque control, field orientation technique is employed to control the PMSM.

Fig. 5 presents the general control scheme of the designed PMSM-based WTE system. A three-phase thyristor bridge rectifier is connected to the grid to provide DC voltage for a three-phase IGBT voltage source inverter. The inverter feeds three-phase power to the motor through space vector pulse width modulation SVPWM. The SVPWM control is provided by the control program executed by the dSPACE DS1104 platform. The PMSM phase currents are measured and mapped in the synchronously rotating frame of reference using the rotor angle measured via an incremental encoder (6000 pulse per turn) embedded in the PMSM. The motor phase currents are controlled such that for all speeds less or equal to the rotor speed, the  $d$ -axis current is maintained zero and

the  $q$ -axis current is maintained at the value that is sufficient to issue the commanded torque. For speeds higher than the rated speed, field weakening is achieved by permitting sufficient amount of the  $d$ -axis current to weaken the rotor magnet flux as desired. In both cases, the machine flux and the developed torque are separately controlled and decoupled from each other which is the major merit of field orientation that resembles the characteristics of a separately excited DC motor.

#### IV. DESIGN PROCEDURE FOR CURRENT LOOPS PI-CONTROLLER

The design procedures for obtaining the PI controller gains for both  $d$ -axis and  $q$ -axis currents are the same for surface-mounted magnet type of PMSM where the stator inductances of the  $d$ - and  $q$ - axis are the same. In order to have a simpler design of the current controllers and to control the  $dq$  currents independently, a decoupling factor from the stator voltage equation must be considered as shown in Fig.6 and Fig. 7.

The design procedure can be achieved by the following steps:

1- The overall open loop transfer function of the  $q$ -axis can be written as:

$$G_{ol}(S) = G_{sam}(S) * G_c(S) * G_{CA}(S) * G_{iq}(S) \quad (7)$$

where  $G_{sam}(S)$  is the current sensor transfer function,  $G_c(S)$  is the PI controller transfer function,  $G_{CA}(S)$  is the transfer function of the control algorithm, and  $G_{iq}(S)$  is the transfer function of the  $q$ -axis current path.

2- The open loop transfer function of the PI controller is:

$$G_c(S) = K_p + \frac{K_i}{S} = K_p \left( \frac{1 + T_i S}{T_i S} \right) \quad (8)$$

where  $T_i = \frac{K_p}{K_i}$  is the integrator time constant.

3- The control algorithm block represents the delay in the digital calculation and its open loop transfer function is:

$$G_{CA}(S) = \left( \frac{1}{T * S + 1} \right) \quad (9)$$

4- The plant ( $q$ -axis current controller loop) has an open- loop transfer function from the  $q$ -axis voltage equation after removing the decoupled part as follows:

$$G_{iq}(S) = \frac{i_q(S)}{V_q(S)} = \frac{1/R}{1 + \frac{L_q}{R} S} = \frac{K_a}{1 + T_q S} \quad (10)$$

where  $T_q$  is the motor electrical time constant and  $T_i = T_q$ .

The sampling block is the delay resulted from the digital to analog conversion (DAC). It is also a first order transfer function with the time constant  $T$ .

$$G_{sam}(S) = \left( \frac{1}{0.5 * T * S + 1} \right) \quad (11)$$

By substituting (8) - (11) into (7), one gets the following:-

$$G_{ol}(S) = \left( \frac{1}{T * S + 1} \right) * \left( \frac{1}{0.5 * T * S + 1} \right) * \frac{K_a}{1 + T_q S} * K_p \left( \frac{1 + T_i S}{T_i S} \right) \quad (12)$$

To simplify the overall transfer function, a time constant is introduced which represents the approximation of all 1<sup>st</sup> order transfer functions that make delays because their values are small compared with the electrical motor time constant, causing smaller dynamics. This implies that the transfer function of the delays will be replaced by a unique transfer function of 1<sup>st</sup> order having a time constant equal the sum of all time constants of the system [12].

$$T_{all} = 1.5 * T \quad (13)$$

Hence, the open loop transfer function of (12) will have a simpler form as follows:

$$G_{ol}(S) = \frac{K_a * K_p}{T_i * S(1 + T_{all} * S)} \quad (14)$$

For obtaining the value of  $K_p$ , it is necessary to use a controller design criterion called Optimal Modulus (OM) with the damping factor selected to be  $\zeta = \frac{\sqrt{2}}{2}$ . The open loop transfer function of a 2<sup>nd</sup> order system has the form of:

$$G_{OM}(S) = \frac{1}{2\zeta * S * (1 + \zeta * S)} \quad (15)$$

If the analogy between (14) and (15) is made, hence, the following relations are deduced in order to determine the gains of the  $I_q$ -PI controller:

$$\frac{K_p * K_a}{T_i} = \frac{1}{2 * T_{all}} \quad (16)$$

$$K_p = \frac{T_i}{2 * K_a * T_{all}} \quad (17)$$

By substituting the values of  $(T_i, K_a, T_{all})$ , one gets the  $K_p$  value as:

$$K_a = \frac{1}{R} = 0.9161, T_i = \frac{L_q}{R} = \frac{3.553563 * 10^{-3}}{0.916} = 0.0039 \text{sec}, T_{all} = 1.5 * 180 * 10^{-6} = 2.7 * 10^{-4} \text{sec} \quad K_p = \frac{0.0039 * 0.9161}{2 * 2.7 * 10^{-4}} = 6.5807$$

(Proportional gain of the  $I_d$  and  $I_q$ ).

And the  $K_i = \frac{K_p}{T_i} = \frac{6.5807}{0.0039} = 1.6964 * 10^3$  (Integral gain of the  $I_d$  and  $I_q$ ).

Substituting the values of  $K_p$  and  $K_i$  into (7):

$$G_c(S) = K_p + \frac{K_i}{S} = 6.5807 + \frac{1.6964 * 10^3}{S} \quad (18)$$

The Equation (18) can be written in the discrete form as follows:

$$G_c(Z) = \frac{6.733 * Z - 6.428}{Z - 1} \quad (19)$$

The performance of the values of  $(K_p$  and  $K_i)$  obtained from the previous calculation and the tuning process is depicted in Fig. 9. The values of the  $(K_p$  and  $K_i)$  after tuning of the current PI-controller are:  $K_p = 8.1401, K_i = 2763.3435$ .

## V. EXPERIMENTAL RESULTS

In this section, the performance of the PMSM-based WTE has been tested experimentally under different conditions. The experimental setup for the wind turbine emulation system is shown in Fig. 10. The Emulator is coupled to another PM machine working as a generator and loaded with a variable resistance. The parameters of PMSM are given at Table II. Several tests have been conducted to check the performance and effectiveness of the wind emulation system. These tests are grouped into two sets. The first one is to check the static behavior of the proposed WTE and its ability to generate the wind torque-speed characteristic. This experiment has done three times with different fixed wind speed. The wind speeds used in the experimental tests of the system are 6, 8, and 9 m/sec. The second one is the test of the dynamic behavior of the proposed system. The system dynamic behavior is tested under different cases. These cases include a sudden change in load under constant wind speed, sudden change in wind speed, and finally system performance using a real site wind speed profile.

### A. Torque-Speed Characteristics at Different Wind Speeds

Within the first set of test, at each wind speed, the resistive load on the PM generator changes from no load to full load to draw the torque-speed characteristic of the emulated turbine and verified against the real wind turbine torque-speed characteristic which is generated from the system simulation on Matlab/Simulink. The exact wind turbine torque-speed characteristic and the torque-speed characteristic of the WTE system implemented using PMSM is shown in Fig. 11.

### B. Dynamic Tests

#### 1) The Sudden Change of Load at Constant Wind Speed

To test the system torque tracking, the resistive load was stepped frequently from no load to a certain random load while the wind speed is set to 8 m/sec. As shown in Fig. 12, the developed torque of the PMSM tracks very well the torque command issued from the wind turbine block. Also, the power coefficient,  $C_p$  increases by increasing the output torque from the motor.

#### 2) Sudden Change of Wind Speed

Another test is conducted to test the dynamic behavior of the system. A step change in wind speed from 6 m/sec to 8 m/sec and back from 8 m/s to 6 m/s is applied to the system with a constant resistance applied to the PMSG. Fig. 13 illustrates the load and WTE torque-speed characteristics. The system initially operates at 6 m/sec at point A shown in Fig. 13 and suddenly the wind speed is increased to 8 m/sec so the operating point of the system moves to B. At point B, the available torque is greater than the load torque imposed by the resistance on the PMSG so the system will accelerate until reaching a new equilibrium point C where the torque and rotor speed are greater than those at point B. The cycle is reversed during the step back from 8 m/s to 6 m/s wind speed. The time which the system takes to reach point C depends on the overall inertia of the rotating mass. In Fig. 14, by changing the wind speed as described earlier, the torque increases and the rotor speed increases when the wind speed is stepped up and decreased when the wind speed is stepped down. The figure shows also the perfect tracking of the motor torque to the torque command.

### 3) WTE System Performance under Stochastic Wind Speed Profile

The main goal of this test is to study the system performance under stochastic wind speed profile. A realistic wind model is vital for a full assessment of the controllers' performance. The realistic wind speed at a certain point can be divided into two significant components, i.e., the average wind speed associated to the macro-meteorological conditions and the turbulence which represents the fast changes of the wind speed. A wind model is usually divided into two time scales, namely  $t_{s1}$  for the average wind speed and  $t_{s2}$  for the turbulence where  $t_{s2} < t_{s1}$  [13]. Fig. 15 outlines a block diagram of the realistic wind speed model. This model is essentially divided into two portions; the average wind speed,  $V_m$ , and the turbulence wind speed,  $v$ . In this paper, the tower shadow and the wind shear components are ignored and a realistic wind speed,  $V_{wind}$ , can be given as follows:

$$V_{wind} = V_m + v \quad (20)$$

The average wind speed is obtained as the average of the instantaneous speed over an interval  $t_p$  as follows [13]:

$$V_m = \frac{1}{t_p} \int_{t_0 - t_p/2}^{t_0 + t_p/2} V(t) dt \quad (21)$$

The averaging period is selected to be within the energy gap shown in Fig.17, more precisely around 10 min to 20 min [13].

#### A. Mean Wind Speed Model

The average wind speed model is presented in [14]. This model depends on the van der Hoven spectrum illustrated in Fig. 16 [15].

The frequency range below  $1/t_p$  is divided into  $m$  intervals. Then, the average wind speed is calculated every  $t_{s1}$  as:

$$V_m(t) = V_0 + \sum_{i=1}^m A_i \cos(\omega_i t + \zeta_i) \quad (19)$$

where  $\omega_i$ ,  $i = 1, \dots, m+1$  is the discretized angular frequency,  $\zeta_i$  is a stochastic variable uniformly distributed in  $[-\pi, \pi]$ ,  $V_0$  is the average speed measured during a period much longer than  $2\pi/\omega_1$  and  $A_i$  is given as follows [13]:

$$A_i = \frac{2}{\pi} \sqrt{\frac{1}{2} (S_v(\omega_i) + S_v(\omega_{i+1})) (\omega_{i+1} - \omega_i)} \quad (19)$$

where  $S_v(\omega_i)$  is the power spectral density (PSD) at  $\omega_i$  as illustrated in Fig. 16.

#### B. Turbulence Model

The wind turbulence is defined by the power spectrum. The power spectrum is characterized by the correlation length, the turbulence intensity and the average wind speed [13]. According to [13] and [16], a turbulence model can be formed by filtering white noise via a low-pass filter having a frequency response of the power spectrum as illustrated in Fig. 17. The low pass filter in [13] is given as follows:

$$H_f(i\omega) = K_v \frac{(i\omega T_v a_1 + 1)}{(i\omega T_v + 1)(i\omega T_v a_2 + 1)} \quad (22)$$

where  $K_v$  is calculated for the filter output  $\omega_c(t)$  to have a unity variance,  $a_1 = 0.4$ , and  $a_2 = 0.25$ , respectively. Recall that  $T_v = L_v/V_m$ , where  $\sigma_v$  and  $L_v$  are obtained experimentally at the location of the wind turbine.

Turbulence is therefore conducted by multiplying the filter output by the estimated standard deviation of the turbulence  $\sigma_v$ . Fig. 18 represents wind speed profile started at  $t = 0.4$  sec. This wind speed profile was constructed with the model described in Fig. 15. The parameters were set to  $L_v = 180$  m,  $\sigma_v = 0.16$ ,  $V_m = 9$  m/sec,  $t_{s1} = 180$  sec, and  $t_{s2} = 1$  sec, respectively [13].

The dynamics of the implemented emulator is tested by applying a real stochastic wind speed profile. As presented in Fig. 19, the rotor speed varies by the wind speed change and the motor torque perfectly tracks the torque command.

## VI. CONCLUSION

A wind turbine emulator has been implemented to reproduce the characteristics of a real wind turbine in the laboratory. A good emulator can afford great flexibility and reduce costs of conducting research on WECS. A PMSM-based wind turbine emulator has been implemented to create a controlled test environment for a practical wind turbine drive train. A lot of tests have been conducted on the proposed system to check the system robustness, immunity, and dynamic performance. The system tracks the torque command issued from a wind turbine block under a sudden change in the applied load to the motor, sudden change in wind speed, and under stochastic wind speed variation. The system precision in emulating the torque-speed characteristics of the target turbine is also verified. This experimental work concludes that the PMSM is the best option to emulate the wind turbine characteristics to be used in the research and development of the wind energy conversion systems.

## REFERENCES

- [1] R. I. Ovando, J. Aguayo, M. Cotorogea, "Emulation of a Low Power Wind Turbine with a DC motor in Matlab/Simulink," PESC'07, Orlando, FL, June 2007, pp. 859 – 864.
- [2] S. Kouadria, S. Belfedhal, E.M. Berkouk, Y. Meslem, "Development of real time wind turbine emulator based on DC motor controlled by PI regulator," *8th International Conference (EVER), Monte Carlo*, March 2013, pp. 1 – 5.
- [3] S. Kouadria, S. Belfedhal, Y. Meslem, E.M. Berkouk, "Development of real time Wind Turbine Emulator based on DC Motor controlled by hysteresis regulator," *International Renewable and Sustainable Energy Conference (IRSEC)*, Ouarzazate, March 2013, pp. 246 – 250.
- [4] Weihao Hu, Yue Wang, Xianwen Song, Zhaoan Wang, "Development of wind turbine simulator for wind energy conversion systems based on permanent magnet synchronous motor," *International Conference on Electrical Machines and Systems*, Wuhan, Oct. 2008, pp. 2322 – 2326.
- [5] Liyong Yang, Sufang Yan, Zhigang Chen, Weipeng Liu, "A novel wind turbine simulator for wind energy conversion systems using an permanent magnet synchronous motor," *International Conference on Electrical Machines and Systems (ICEMS)*, Busan, Oct. 2013, pp. 2156 – 2158.
- [6] H. Voltolini, M.H. Granza, J. Ivanqui, R. Carlson, "Modeling and simulation of the Wind Turbine Emulator using induction motor driven by torque control inverter," *10th IEEE/IAS International Conference on Industry Applications (INDUSCON)*, Fortaleza, Nov. 2012, pp. 1 – 6.
- [7] A.G. Abo-Khalil, "A new wind turbine simulator using a squirrel-cage motor for wind power generation systems," *IEEE Ninth International Conference on Power Electronics and Drive Systems (PEDS)*, Singapore, Dec. 2011, pp. 750 – 755.
- [8] W. Li, D. Xu, W. Zhang, H. Ma., "Research in wind turbine emulation based on DC motor," in *2nd IEEE conference industrial Electronics and Applications*, 2007, pp. 2589-2593.
- [9] T. Thiringer and J. Linders, "control by variable rotor speed of a fixed pitch wind turbine operating in a wide speed range," *IEEE trans. energy conv.*, Vol. 8, pp. 520–526, Sept. 1993.
- [10] J.D.M. De Kooning, B. Meersman, T.L. Vandoorn, L. Vandeveldel, "Evaluation of the Maximum Power Point Tracking performance in small wind turbines," *IEEE Power and Energy Society General Meeting*, San Diego, CA, pp. 1 – 8.
- [11] Cesar Hernaez, "Sensorless speed and position estimation of a PMSM," Master Thesis, Aalborg University, Department of Energy Technology, 2014.
- [12] [http://dsp.vscht.cz/konference-Matlab/Matlab10/full\\_text/070\\_Mina](http://dsp.vscht.cz/konference-Matlab/Matlab10/full_text/070_Mina)
- [13] F. D. Bianchi, H. De Battista, R. J. Mantz, and O. D. Bianchi, *Wind turbine control systems: Principles, modeling and gain scheduling design*. London: Springer London, 2006.
- [14] C. Nichita, D. Luca, B. Dakyo and E. Ceanga, "Large band simulation of the wind speed for real time wind turbine simulators", *IEEE Transactions on Energy Conversion*, vol. 17, no. 4, pp. 523-529, 2002.
- [15] I. Van der Hoven, "Power Spectrum of Horizontal Wind Speed in The Frequency Range from 0.0007 To 900 Cycles per Hour", *Journal of Meteorology.*, vol. 14, no. 2, pp. 160-164, 1957.
- [16] E. Welfonder, R. Neifer and M. Spanner, "Development and experimental identification of dynamic models for wind turbines", *Control Engineering Practice*, vol. 5, no. 1, pp. 63-73, 1997.



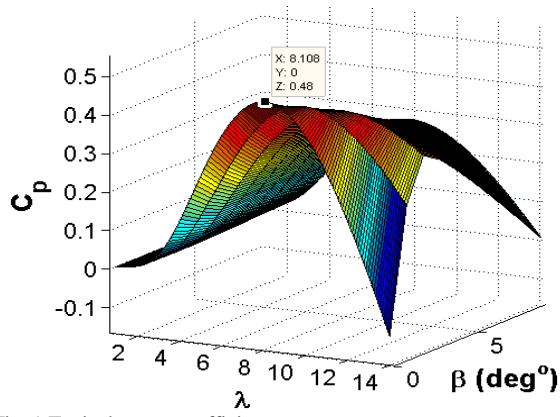


Fig. 1 Typical power coefficient curve

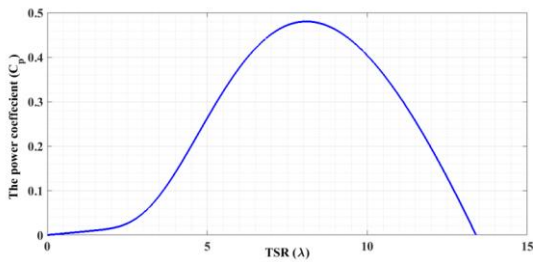


Fig. 2 Typical power coefficient curve (at  $\beta = 0$ )

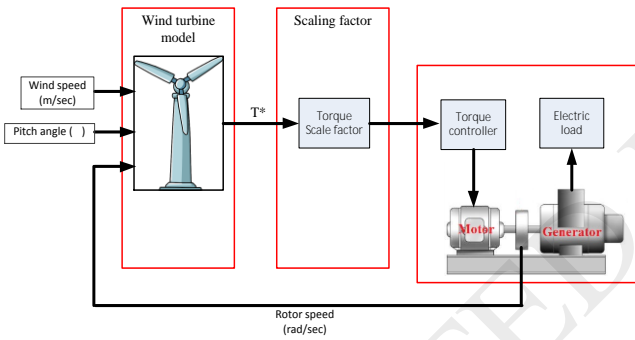


Fig. 3 Complete strategy of emulating wind power

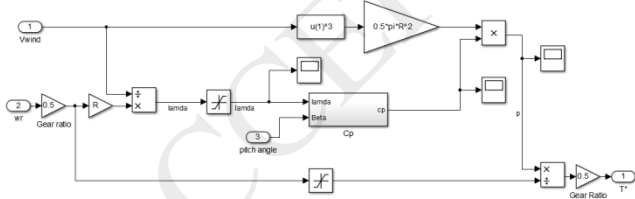


Fig.4 Three-KW Wind turbine Matlab/Simulink model

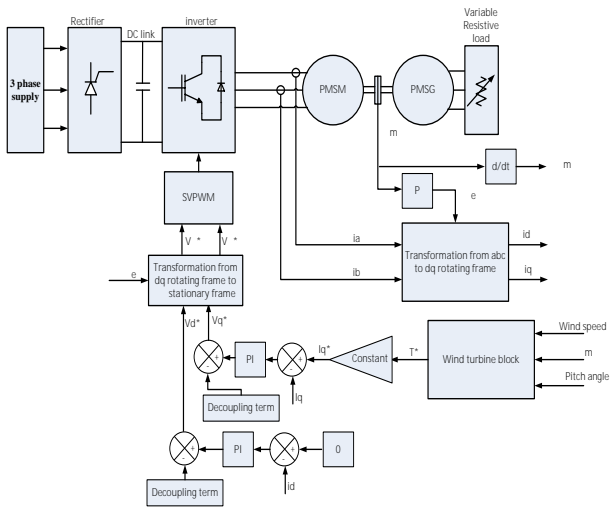


Fig.5 General control scheme of PMSM-based WTE system

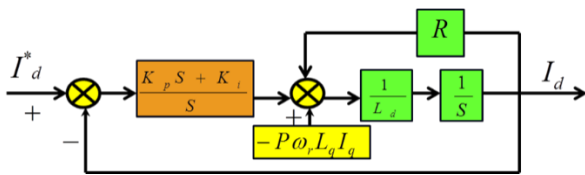


Fig. 6 Current loop controller of PMSM in the  $d$ -axis

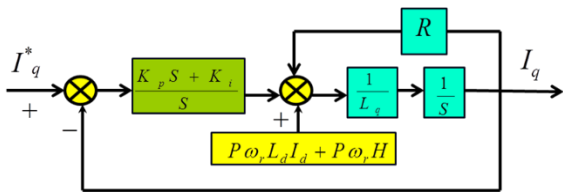


Fig. 7 Current loop controller of PMSM in the  $q$ -axis

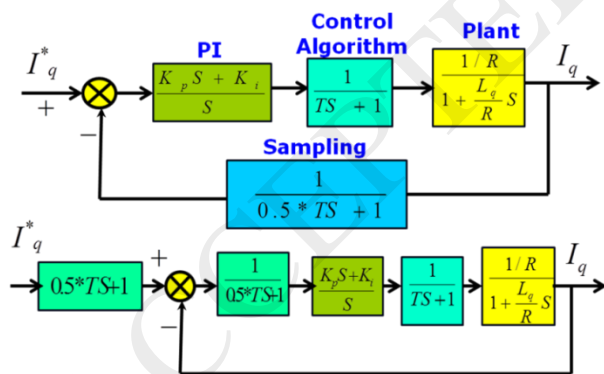


Fig. 8 Current loop controller of PMSM in  $q$ -axis with unity feedback

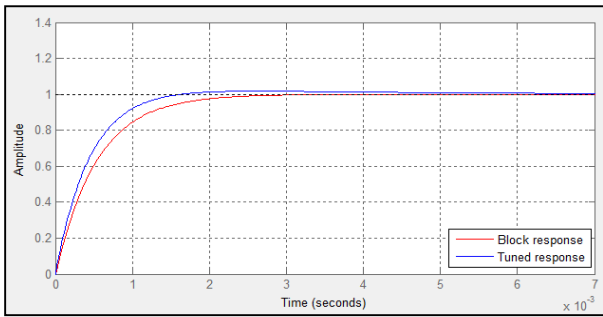


Fig. 9 Tuned response of PI<sub>Iq</sub> controller



Fig. 10 Experimental setup for WTE using PMSM loaded with PMSG

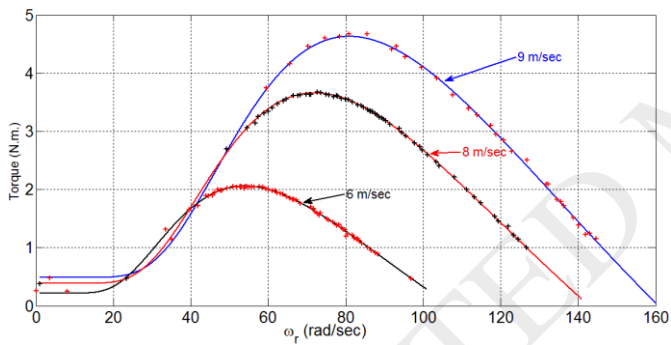


Fig. 11 Torque speed characteristic of wind turbine simulation and real time WTE using PMSM

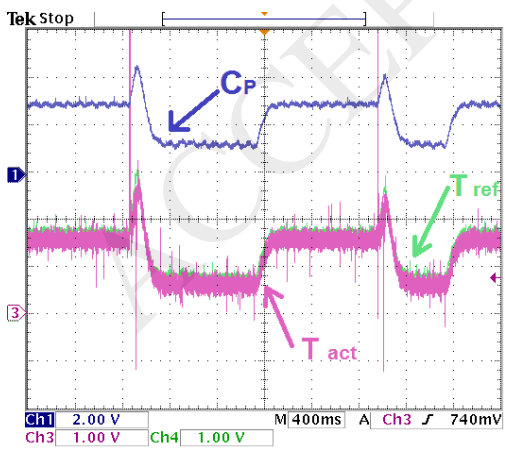


Fig. 12 WTE behavior under load change at constant wind speed

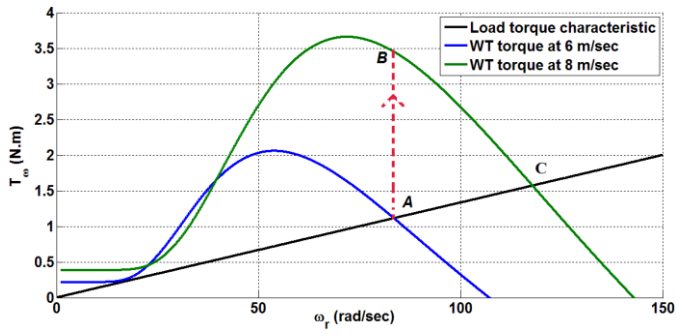


Fig. 13 load characteristic and wind turbine characteristic at wind speeds 6 and 8 m/sec

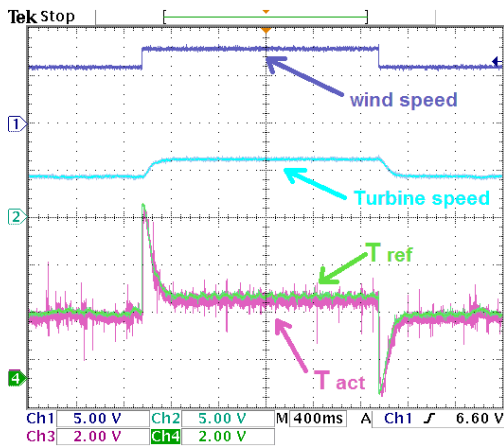


Fig. 14 PMSM-based WTE behavior under sudden wind speed change from 6 m/sec to 8 m/sec.

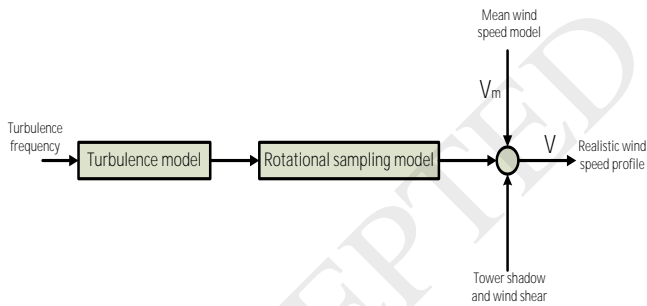


Fig. 15 Block diagram of the realistic wind model

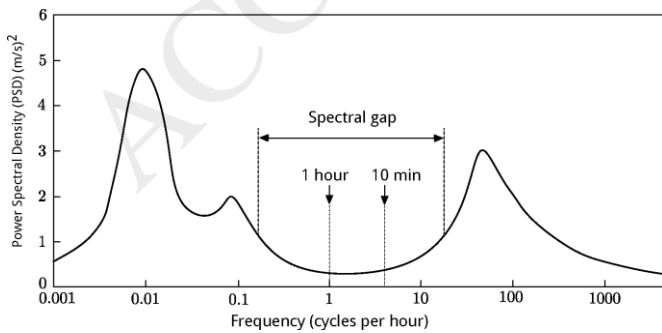


Fig. 16 Typical van der Hoven spectrum [15]

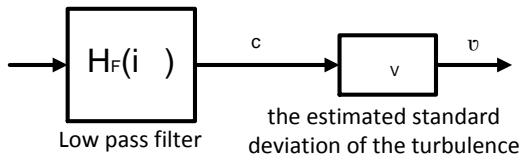


Fig. 17 The turbulence wind model [13]

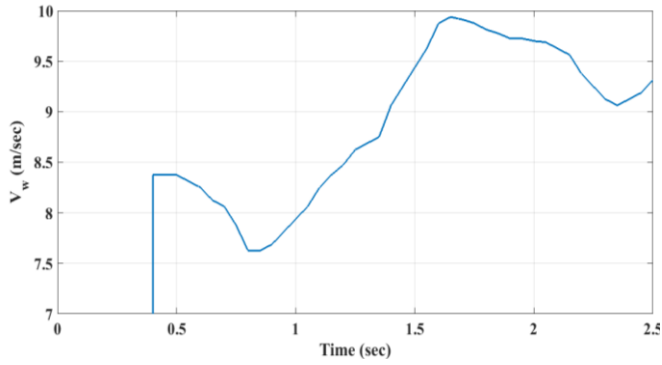


Fig.18 Stochastic wind speed profile

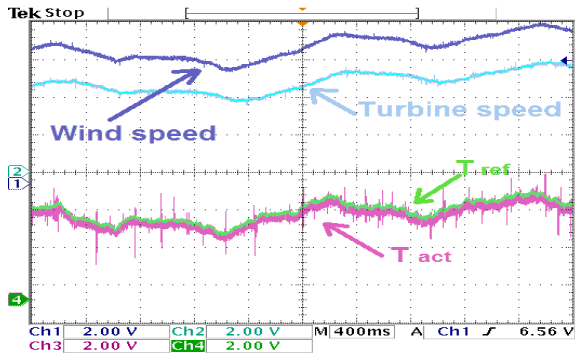


Fig. 19 PMSM-based WTE behavior under stochastic wind speed profile

Table I  
PARAMETERS OF THE POWER COEFFICIENT EQUATION

| $C_1$  | $C_2$ | $C_3$ | $C_4$ | $C_5$ | $C_6$  |
|--------|-------|-------|-------|-------|--------|
| 0.5176 | 116   | 0.4   | 5     | 21    | 0.0068 |

Table II  
PMSM PARAMETERS

|               |          |              |           |
|---------------|----------|--------------|-----------|
| Rated speed   | 1500 rpm | Rated torque | 5.649 N.m |
| Rated current | 2.6 A    | Peak torque  | 15.2 N.m  |
| Rated voltage | 230 V    |              |           |

ACCEPTED MANUSCRIPT